Journal of the Mechanics and Physics of Solids 70 (2014) 62–70

Contents lists available at ScienceDirect

Journal of the Mechanics and Physics of Solids

journal homepage: www.elsevier.com/locate/jmps

Grain boundaries in hybrid two-dimensional materials

Zhuhua Zhang, Yang Yang, Boris I. Yakobson *

Department of Materials Science and Nanoengineering, Department of Chemistry, and the Smalley Institute for Nanoscale Science and Technology, Rice University, Houston, TX 77005, United States

ARTICLE INFO

Article history:
Received 7 January 2014
Received in revised form
14 April 2014
Accepted 12 May 2014
Available online 21 May 2014

Keywords:
Grain boundary
Two dimensional material
Hybrid material
Dislocations
First-principle calculations

ABSTRACT

In two-dimensional (2D) materials, bisector grain boundaries (GBs) are energetically favorable as they allow perfect match of neighbor grains. We demonstrate here a contrasting behavior for GBs in hybrid 2D materials, which tend to be non-bisector and obey a universal law to optimally match the heterogeneous grains: the ratio of cosines of the rotation angles of two neighbor grains equals the ratio of constituent's lattice parameters, reminiscent of Snell's law for light refraction. Details of the optimal GB structures are further formulated in terms of tilt angle, lattice mismatch strain and deviation angle from the bisector line, in good agreement with comprehensive numerical analyses. The ground state structures of the GBs manifest as a series of laterally misaligned bisector segments, which are verified by intensive first-principle calculations. Our findings not only provide a general guidance for exploring GBs in various hybrid 2D materials but also serve as an important stepping stone for understanding mechanical and electronic behaviors in these 2D nanoscale patchworks.

1. Introduction

In the past few years, two-dimensional (2D) materials have undergone a flurry of research activities, leading the science and technology for low-dimensional materials into a 2D age. Among various 2D materials synthesized thus far, graphene (Novoselov et al., 2005; Zhang et al., 2005; Castro Neto et al., 2009) and single-layered hexagonal boron nitride (h-BN) (Geim and Novoselov, 2007). have attracted considerable research attention, not only owing to similar hexagonal honeycomb lattices but also because of their supreme mechanical properties (Lee et al., 2008; Chang and Gao, 2003; Chang et al., 2006). However, graphene is a zero-gap semi-metal, while the h-BN monolayer is electrically insulating with a wide band gap of ~5.8 eV (Nag et al., 2010; Golberg et al., 2010; Zhang and Guo, 2008; Jin et al., 2009; Jiang and Guo, 2011). The distinct properties of the two hexagonal isologues have stimulated great interests in fabricating hybridized atomic layers composed of graphene and BN domains—a new 2D BNC material with properties complementary to those of its constituents (Ci et al., 2010; Sutter et al., 2012; Liu et al., 2011, 2013; Gao et al., 2013). Of most interest is the fact that varying the ratio of composition could endow the hybrid BNC sheet with tunable band gap on-demand, ranging from 0 eV to 5.8 eV (da Rocha Martins and Chacham, 2010; Ramasubramaniam and Naveh, 2011; Bhowmick et al., 2011; Jung et al., 2012; Muchharla et al., 2013; Ding et al., 2009; Lu et al., 2011; Lu et al., 2010). Moreover, having BN domains patched in otherwise perfect graphene structures leads to appearance of edge states localized at the BN/graphene interfaces, enabling the advent of spin-polarization (Ramasubramaniam and Naveh, 2011; Lu et al., 2010) and even possible half-metallicity

* Corresponding author.
E-mail address: biy@rice.edu (B.I. Yakobson).

http://dx.doi.org/10.1016/j.jmps.2014.05.009
0022-5096/

(Dutta et al., 2009; Liu et al., 2011). All these colorful properties, however, are closely correlated with the interface between the graphene and BN domains, which is at the center of the study of hybrid 2D materials (Ajayan and Yakobson, 2011). Having a clear picture towards understanding the hybrid interface will not only provide essential basis for further study of fundamental physics and potential applications but also help understand the growth mechanism of the nanoscale patchworks. Unfortunately, limited by related techniques in preparation and characterization, experimental images of atomically sharp BNC interfaces remain rather scarce thus far.

Prior to experimental observation, insightful theoretical study on the hybrid interfaces is appealing. All previous theoretical works on the 2D BNC sheets are based on epitaxial interfaces, that is the BN and graphene domains are stitched in a way that the honeycomb lattice can be continuous across the interfaces, mostly manifesting as zigzag- and armchair-shaped interfaces (Bhowmick et al., 2011; Jung et al., 2012; Dutta et al., 2009; Liu et al., 2011). The epitaxial interfaces, however, may be far from the real situation in experiments, in view of the following two aspects. First, epitaxial interfaces impose significant in-plane strains on all the domains due to considerable lattice mismatch between graphene and h-BN. As the in-plane strain is non-decaying, the epitaxial interfaces rapidly raise the system energy with increasing domain sizes, rendering them unfavorable choice. Second, in real process, graphene and BN domains can be nucleated at different sites on substrates (Liu et al., 2013). If the domains are misoriented with each other, their growth and coalescence lead to formation of dislocations and grain boundaries (GBs), which are found to be ubiquitous in 2D materials. While GBs have been extensively studied in graphene and h-BN (Kim et al., 2011; Huang et al., 2011; Yu et al., 2011; Liu and Yakobson, 2010; Yazyev and Louie, 2010; Liu et al., 2012; Gibb et al., 2013; Wei et al., 2012; Wu and Wei, 2013; An et al., 2011), they have never been addressed in related hybrid materials. Several fundamental questions are raised naturally: is it possible to lift the

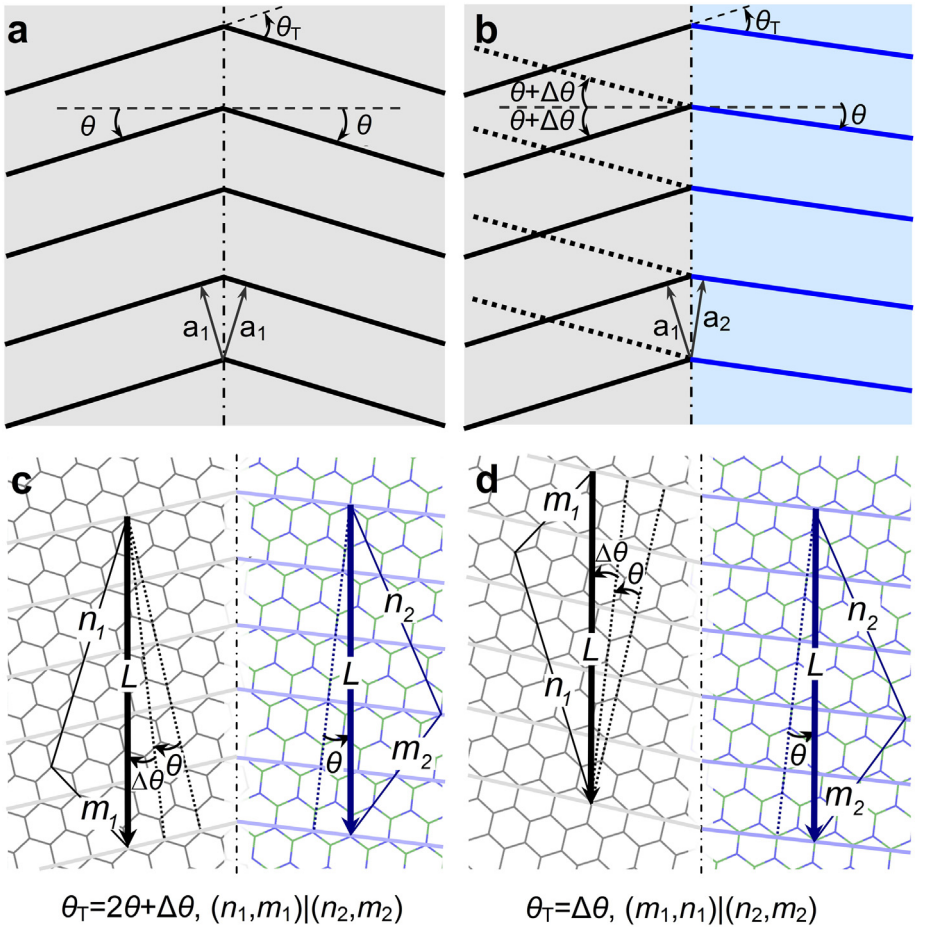

Fig. 1. Preferred grain boundaries (GB) in 2D materials. (a) Schematic model of a bisector GB in a homogenous 2D material, with the left and right domains symmetrically rotated by θ. The tilt angle of GB is $\theta_T=2\theta$. (b) Schematic model of a GB in a hybrid martial perfectly matching domains 1 and 2, for which only lattice rows are shown. Given a rotation angle θ for the domain 2, there are two alternative rotation angles $\theta+\Delta\theta$ and $-\theta-\Delta\theta$ for the domain 1, as shown by black solid and dotted lines. a_1 and a_2 are the lattice constants of the domains 1 and 2, respectively. Applying the scheme shown in (b) into the GB in 2D BNC sheet at tilt angles of (c) $2\theta+\Delta\theta$ and (d) $\Delta\theta$. The repeat vectors, denoted by thick solid lines with arrow, are (n_1,m_1) for the domain 1 and (n_2, m_2) for the domain 2, both having a length L. Dotted lines illustrate how the repeat vectors are rotated from the armchair direction. C, B and N are distinguished in gray, green and blue, respectively. (For interpretation of the references to color in this figure legend, the reader is referred to the web version of this article.)

lattice mismatch by regulating the GBs in hybrid 2D materials? If that were the case, what physical law governs this regulation and what atomic organizations emerge with the GBs?

In homogenous materials, GBs are energetically more favorable when bisecting the angle between the crystallographic orientations of the two domains (see Fig. 1a) (Liu and Yakobson, 2010), allowing the domains to get rid of in-plane strain. Bisector GBs for hybrid 2D materials will cause additional strain energy, attributed to the lattice mismatch. Instead, the GBs have to deviate from the bisector line for realizing the optimal match of grains. However, setting up a general law to describe the optimally matched GBs in hybrid 2D materials encounters difficulties in combinatorics among the lattice orientations, mismatch and periodicity. Toward solving this issue, an inspiration comes from a well-known physical phenomenon associated with interfaces between two media, through which a ray of light undergoes a change in its wave length as well as its refraction angle from incidence. A simple formula, known as Snell's law, describes the relationship among the incidence and refraction angles and wave lengths of light. If we regard the incidence and refraction angles as the rotation angles of domains and the light wave length as the "lattice constants", a similar law for lattices at GBs in hybrid 2D materials can be envisioned. Indeed, here, our comprehensive analyses reveal that two heterogeneous domains in hybrid 2D materials can be optimally matched with no in-plane strain once the ratio of cosines of the rotation angles of the two domains is equivalent to the ratio of their lattice constants. Based on this law, the details of GB structures are determined via optimal combination of misorientation angle, lattice mismatch and periodic length of GBs and energetically confirmed by first-principle calculations. Our study represents the first effort to address the GBs in hybrid 2D materials and may shed light on understanding their mechanical behaviors and functions.

2. Analytical results

For generality of our analyses, we consider a hybrid 2D material composed of domain 1 with lattice constant a_1 and domain 2 with lattice constant a_2 (Fig. 1b). The corresponding lattice mismatch is $\varepsilon=(a_2-a_1)/a_1$ $(a_2>a_1)$. The rotation angle between the crystallographic orientation and the normal of the boundary line is $\theta+\Delta\theta$ for the domain 1, and θ for the domain 2. The atomic arrangement around the GB not only depends on its tilt angle $\theta_T=2\theta+\Delta\theta$, but also on $\Delta\theta$ and ε. Since direct consideration of numerous possibilities cannot be afforded, a preliminary analysis is useful for screening. A prerequisite for the optimal match is that all the lattice rows in the hybrid 2D material should continuously cross the GB (Fig. 1c); otherwise additional dislocations or imperfections must be included to accommodate the lattice rows disconnected at the GB and raise the system energy. GBs satisfying this condition will be in priority and the main choice for detailed analyses. Nevertheless, other GBs out of this condition, if formed in the course of growth, can be kinetically stabilized and encountered in observations as well. With these provisions, we can derive the relation between rotation angles and ε. Fig. 1b shows a simplified model of two stitched domains, with only lattice rows being presented. Perfect match of the lattice rows across the GB requires that the projections of two domains' lattice constants onto the GB line are equal, so $a_1/\cos(\theta+\Delta\theta)=a_2/\cos(\theta)$, further expressed as

$$\frac{\cos\theta}{\cos(\theta+\Delta\theta)}=1+\varepsilon. \tag{1}$$

Eq. (1) just resembles the equation of Snell's law for describing light refraction. Solving Eq. (1) yields two nonequivalent solutions: $\theta+\Delta\theta$ versus θ and $-\theta-\Delta\theta$ versus θ, as shown by the solid and dashed lines in the domain 1, respectively (Fig. 1b). The corresponding GBs have tilt angles $\theta_T=2\theta+\Delta\theta$ and $\Delta\theta$, respectively. The two types of GBs can be interconverted by a 180° flip of the domain 1 or 2 around the in-plane normal of the GB (Fig. 1c and d). As the geometrical analyses of the two groups of GBs are essentially the same, we focus on the GBs corresponding to the first solution. To further formulate the interdependence of structural parameters in the GBs, we take $\theta=\theta_T/2-\Delta\theta/2$ and $\theta+\Delta\theta=\theta_T/2+\Delta\theta/2$; then Eq. (1) can be rewritten as $\cos(\theta_T/2-\Delta\theta/2)=(1+\varepsilon)\cos(\theta_T/2+\Delta\theta/2)$, which results in

$$\tan\frac{\Delta\theta}{2}=\frac{\varepsilon}{(2+\varepsilon)\tan(\theta_T/2)}. \tag{2}$$

Since $\Delta\theta/2$ is quite small, Eq. (2) can be further simplified as

$$\Delta\theta=\frac{\varepsilon}{(1+\varepsilon/2)\tan(\theta_T/2)}. \tag{3}$$

Eq. (3) presents proportionality between $\Delta\theta$ and the lattice mismatch ε, indicating that the optimal GB with larger ε will be deviated more from the bisector line. In contrast, $\Delta\theta$ increases with decreasing tilt angle θ_T. There is an extreme case at $\theta_T=0$, at which $\Delta\theta$ has no solution. In this case, the GB becomes an epitaxial interface, but dislocations oriented perpendicular to the GB line must be embedded to lift the lattice mismatch. The structure of GBs at this extreme will be a topic for future study and in this study we focus on common tilt GBs.

3. Numerical results

We then numerically analyze the GBs in hybrid 2D materials with specific lattice mismatch. Fig. 1c presents the graphene and BN domains that are misoriented with each other. The GBs in-between the domains break the lattice periodicity intrinsic to the pristine materials. The periodicities of the domains 1 and 2 along GBs now are defined by repeat vectors

(n_1,m_1) and (n_2,m_2), respectively, which satisfy commensurability condition for reaching perfect match. This is similar to the concept of coincidence site lattice for describing GBs in conventional bulk materials (Ranganathan, 1996). For ease of discussion, the GB constructed by repeat vectors (n_1,m_1) and (n_2,m_2) is tagged as $(n_1,m_1)\|(n_2,m_2)$. In Fig. 1c, by applying an elementary law of sines to the triangle in the domain 1, we have

$$\frac{m_1 a_1}{\sin(30^o-\theta-\Delta\theta)}=\frac{n_1 a_1}{\sin(30^o+\theta+\Delta\theta)}=\frac{L}{\sin\ 120^o}. \tag{4}$$

On the other side, from the triangle in the domain 2, we have

$$\frac{m_2 a_2}{\sin(30^o-\theta)}=\frac{n_2 a_2}{\sin(30^o+\theta)}=\frac{L}{\sin\ 120^o}, \tag{5}$$

where L is the length of repeat vectors in both the domains. We thus have the following relation:

$$\begin{aligned} n_2 &= \frac{\sin(30^o+\theta)}{\sin(30^o+\theta+\Delta\theta)(1+\varepsilon)}n_1,\\ m_2 &= \frac{\sin(30^o-\theta)}{\sin(30^o-\theta-\Delta\theta)(1+\varepsilon)}m_1. \end{aligned} \tag{6}$$

We actually cannot directly get solution from Eq. (6), because n_1, n_2, m_1 and m_2 are discrete integers and the lengths of two repeat vectors are unlikely to coincide. Numerical analyses thus become necessary to obtain the optimal match. According to our preceding preliminary analysis, the repeat vectors must satisfy $n_1+m_1=n_2+m_2$, which make sure that all the lattice rows can be connected when crossing the GB (see Fig. 1c and d). Given a repeat vector of one domain, Eq. (6) enables us to approximately get the repeat vector of another domain and to build up the $(n_1,m_1)\|(n_2,m_2)$ GB. For the hybrid BNC sheet with $\varepsilon=1.8\%$, we find that a given (n,m) of the domain 2 is matched most closely by $(n+1,m-1)$ of the domain 1, forming a match regime of $(n+1,m-1)\|(n,m)$. However, the discrete character of $(n+1,m-1)$ and (n,m) results in a residual strain $\varepsilon_R=|L_2-L_1|/L_1$ for the GB, where L_1 and L_2 are lengths of the repeat vectors in the domains 1 and 2, respectively. At a given rotation angle θ of the domain 2, the residual strain changes with varying periodic length L, taken as $(L_1+L_2)/2$, and should disappear in the optimal GB with an optimal L. To further clarify this point, we show in Fig. 2a (a 2D plot is shown in Fig. S1) the residual strain ε_R as functions of L for four groups of BNC GBs with differently fixed θ. With varying L, ε_R can be

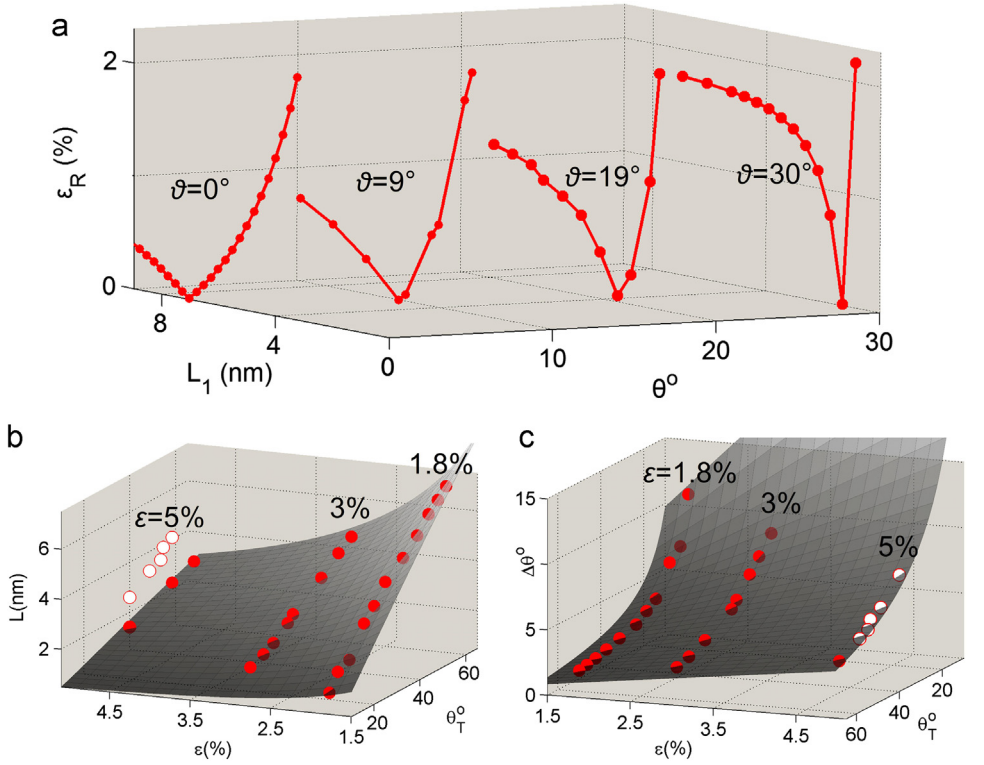

Fig. 2. Structural parameters of the optimal GBs in hybrid 2D materials. (a) Residual strain ε_R in GBs with differently fixed θ in the 2D BNC sheet as functions of the periodic length L of GB; all the GBs follow the $(n+1,m-1)\|(n,m)$ regime. (b) L and (c) $\Delta\theta$ as functions of tilt angle θ_T in the optimal GBs. The results with filled symbols are for GBs constructed by a regime of $(n+1,m-1)\|(n,m)$, while those with red hollow circles at $\varepsilon=5\%$ are for GBs by a regime of $(n+1,m-2)\|(n,m)$, in which both grains are tilted from the zigzag direction. Symbols show numerical results while dark gray 3D plots are analytical solutions. (For interpretation of the references to color in this figure legend, the reader is referred to the web version of this article.)

minimized to nearly zero in all the curves; the optimal L for the minimum ε_R decreases with decreasing θ. The corresponding optimal GBs in the 2D BNC sheet turn out to be (4,2)‖(3,3), (11,4)‖(10,5), (19,3)‖(18,4) and (29,−1)‖(28,0) at $\theta=30^\circ$, 20°, 10°, and 0°, respectively. Similar numerical analyses can be applied to determine the optimal GBs at other tilt angles as well as at $\varepsilon=3\%$ and 5%. The interdependence among $\Delta\theta$, tilt angle θ_T, and periodic length L in the numerically derived optimal GBs is shown by symbols in Fig. 2b and c. The optimal GB with a smaller θ_T favors a larger $\Delta\theta$, in good agreement with the analytical results from Eq. (3) (shown by 3D dark gray plot in Fig. 2c). In contrast, the periodic length L increases with increasing tilt angle θ_T for all examined ε (Fig. 2b). By a series of geometrical derivation, we also obtain an analytical relationship between L and θ_T as $L\varepsilon=a_2\sin(\theta_T/2)/\cos(\Delta\theta/2)$ (see Fig. S2 in SI). Since $\Delta\theta/2$ is very small and $\cos(\Delta\theta/2)\approx 1$, we have

$$L\approx a_2\ \sin(\theta_T/2)/\varepsilon. \tag{7}$$

Again, the analytical results by Eq. (7) are in excellent agreement with the numerical results shown by dark gray 3D plot in Fig. 2b.

Interestingly, when the length of repeat vector is below 2 nm, the GB switches from the $(n+1,m-1)\|(n,m)$ regime to $(n-1,m+2)\|(n,m)$ regime at $\varepsilon=5\%$, as shown by hollow symbols in Fig. 2b and c, following an increase of L. The $(n-1,m+2)\|(n,m)$ GBs are rotated from zigzag orientation and their tilt angles are thus reversed with respect to 60° (see Fig. S3 in SI). The switch of match regime can be understood based on Eqs. (3) and (7). As the lattice mismatch ε increases and L declines, $\Delta\theta$ increases sharply and cannot be afforded by the $(n+1,m-1)\|(n,m)$ regime, thus resulting in a large residual strain ε_R at all times. Switching to $(n-1,m+2)\|(n,m)$ just accommodates the increased $\Delta\theta$, and then ε_R can be minimized to nearly zero again with increasing L, which now is expressed as $\sqrt{3}a_2\sin(\theta_T/2)/\varepsilon$. Note that $\varepsilon=3\%$ corresponds to a hybrid graphene/graphane sheet (Balog et al., 2010), but $\varepsilon=5\%$ lacks correspondence to real materials, shown here only for information. All the analyses can be applied for the $(m_1,n_1)\|(n_2,m_2)$ GBs corresponding to the second solution of Eq. (1), yielding similar results.

4. Structural details of grain boundaries and first-principle verification

The above analyses have established the framework of optimal GBs in hybrid 2D materials. Now we turn to explore the details of the GB structures. It has been established that GBs in graphene are strings of pentagon–heptagon (5|7) edge dislocations (Huang et al., 2011; Liu and Yakobson, 2010; Gibb et al., 2013). The identical edge dislocations energetically favor a vertical alignment to form a bisector GB. Nevertheless, the optimal GB in hybrid 2D materials is deviated by $\Delta\theta/2$ from the corresponding bisector line. As $\Delta\theta/2$ is quite small (see Fig. 2c), the dislocations will locally form bisector segments and kinks must be embedded to accommodate the deviation. This renders the optimal GB as a kinked line comprised of a series of misaligned bisector segments, which locally have a tilt angle of $\theta_T+\Delta\theta$. For low-angle GB, the dislocation density in each bisector segment is $2\sin(\theta_T/2+\Delta\theta/2)$ (Hirth and Lothe, 1982). With these guidelines, we show in Fig. 3 the atomic structures for several typical GBs in the BNC sheet. Each bisector segment just stands for a repeat unit of the GBs and increases in length with increasing θ_T, following an increase in dislocation density, in line with our analytical results. According to Eqs. (2) and (7), the lateral deviation by the kink is $L\sin(\Delta\theta/2)=a_2/(2+\varepsilon)$, the minimum dislocation can laterally shift from a bisector GB (see Fig. 3).

To verify the ground states of the GB structures, we perform density functional theory calculations as implemented in VASP code (Kresse and Hafner, 1994; Kresse and Furthmüller, 1996), using the projector-augmented wave method for the core region and spin-polarized density functional theory (DFT) based on the generalized gradient approximation (GGA) of Perdew–Burke–Ernzerhof with a plane-wave kinetic energy cutoff of 400 eV. A vacuum layer of 16 Å isolates neighboring periodic images and the Brillouin zone is sampled by 6–12 k-points, depending on the supercell size. The GB energies were calculated using an extended model with periodic boundary conditions containing a pair of complementary GBs, while the relative formation energies of GBs associated with dislocation gliding and pseudo-climbing were examined based on a nanoribbon model (6 nm in width, edge passivated by hydrogen) containing a single GB. The distance between two complementary GBs is 4 nm, while the supercell size along the GB is defined by the repeat vectors. All atomic positions are relaxed using conjugate-gradient techniques until the force on each atom is less than 0.01 eV/Å. We focus on the 2D BNC sheets in view of the extensive experimental interests. As shown above, the length of repeat vectors increases with increasing tilt of the optimal GB, so we can only afford the computations on GBs with small tilt angles. First, we investigate the preferred chemical stoichiometry of dislocations composed of B, N and C atoms. The atomic stoichiometry of dislocations is adjusted by transversely shifting the interface through the dislocations, so as to vary the composition of dislocations from full BN to full carbon. We define a distance d between the interface and the dislocation center to characterize the composition variation (see inset in Fig. 4b). Taking the (4,2)‖(3,3) GB as an example, we compare the formation energies of the GBs with changing chemical compositions. The formation energy is defined as

$$E_f=E_x-E_0+N_{BN}\mu_{BN}-N_C\mu_{BN} \tag{8}$$

where E_x and E_0 are the energies of examined and referenced structures (the reference structure is set as the one with minimum E_f), respectively, μ_{BN} and μ_C are the chemical potentials of BN atomic pair and C atom, N_{BN} is the difference of BN pairs between the examined and referenced structures and N_C is the corresponding difference of C atoms. μ_{BN} and μ_C are chosen as the energies of BN pair and C atom in the single-layered h-BN sheet and graphene, respectively. The results show

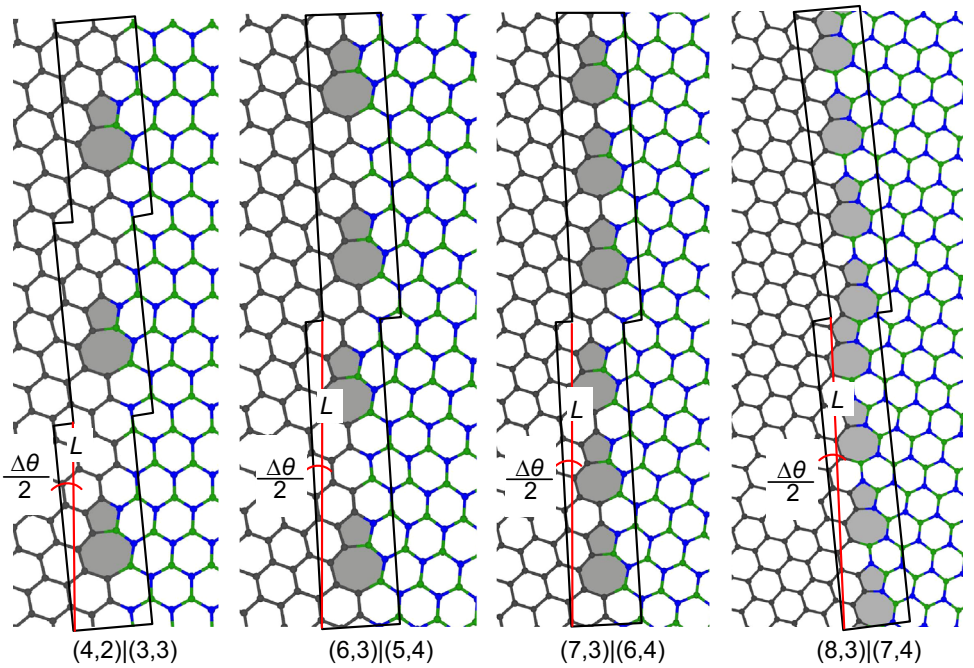

Fig. 3. Ground state atomic structures of optimal GBs in hybrid BNC sheet. Atomic structures of the (4,2)|(3,3), (6,3)|(5,4), (7,3)|(6,4) and (8,3)|(7,4) GBs. The GBs manifest as a kinked line consisting of misaligned bisector segments, and each segment is just the repeat unit of the GB and tilted by $\Delta\theta/2$ from the whole GB direction (along red line). C, B and N are distinguished in gray, green and blue, respectively. (For interpretation of the references to color in this figure legend, the reader is referred to the web version of this article.)

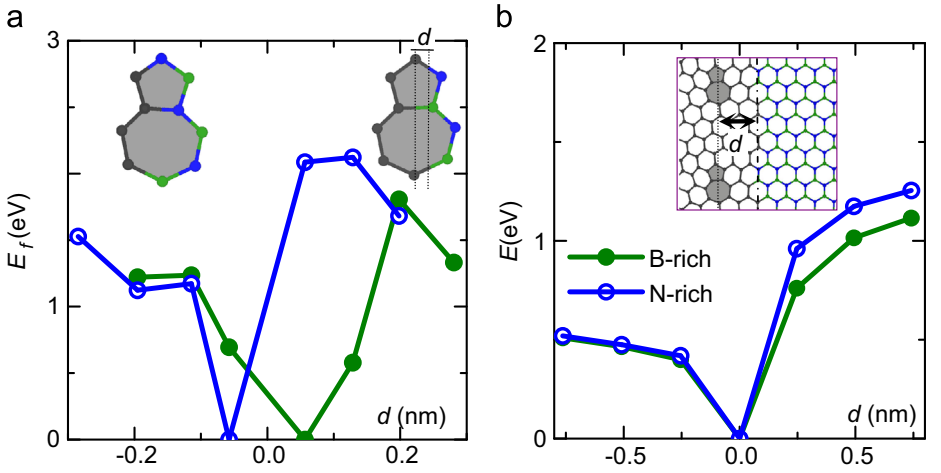

Fig. 4. (a) Formation energy of the (4,2)|(3,3) GB as a function of distance between the BN–C interface and the dislocation center line, as illustrated by the insets. The left and right insets show the most favorable structures for dislocations in N-rich and B-rich GBs, respectively. (b) Relative energy of the (4,2)|(3,3) GB as a function of the distance d between the BN–C interface and the gliding dislocations (dash dot line, see inset).

that the formation energies of both the B-rich and N-rich GBs show a sharp minimum with varying chemical compositions (Fig. 4a). At the minimum, the interface in B-rich GB shifts by ~0.2 nm toward the graphene side while that in N-rich GB shifts in an opposite way (see insets in Fig. 4a). The two types of most favorable GBs have a common feature in that the dislocations are composed of N-rich pentagon and B-rich heptagon. This is because the radius of N atom is smaller than that of C atom and could alleviate compressive stress in pentagon while the larger B atom releases the tensile stress in heptagon. Meanwhile, we find that the length of interface between BN and graphene domains should be minimized for reaching an optimal GB; in this sense, any separation of B and N atoms from the BN domain or separation of C atoms from the graphene domain leads to much higher formation energy (see Fig. S4). The revealed optimal stoichiometries of dislocations are used in all the following calculations. Second, we examine the interaction between the GB and the epitaxial interface where the graphene and BN domains join together. For this purpose, we shift the (4,2)|(3,3) GB relative to the epitaxial interface by gliding all dislocations and find that the total energy sharply increases as the dislocations become farther from the interface

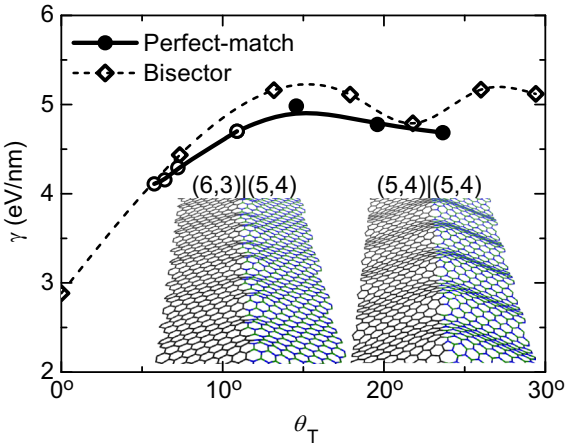

Fig. 5. Energy of optimal (solid line) and bisector (dashed line) GBs in the 2D BNC sheet as functions of tilt angle θ_T. Solid line with hollow circles is for $(m-1,n+1)\|(n,m)$ GBs while that with filled circles is for $(n+1,m-1)\|(n,m)$ GBs. The insets show the relaxed structures of a (6,3)|(5,4) optimal GB and a (5,4)|(5,4) bisector GB.

(Fig. 4b). Therefore, the dislocations and interface are attractively coupled and tend to be superimposed. The underlying reason is that the dislocations can have the stress field relieved to a higher extent when located at the interface, where the bonds are weaker than those in bulk lattices. Third, we perturb the (7,3)|(6,4) GB by gliding a dislocation near the kink, and find the formation energy of GB is increased at least by 1.36 eV/supercell (Fig. S5a); pseudo-climbing the dislocation in the "5" direction by removal of C_2 or a BN dimer also causes energy increase up to 1.71 eV (see Fig. S5b). Finally, we considered several wiggly-shaped (7,3)|(6,4) GBs, which are found to be much less stable than the optimal GBs due to the increase of both the amount of dislocations and the length of BN–C interface (not shown).

Can the optimal GBs be more favorable than commonly supposed bisector structures? Fig. 5 summarizes the energies for a set of $(n+1,m-1)\|(n,m)$ and $(m-1,\ n+1)\|(n,m)$ optimal GBs in the 2D BNC sheet, together with $(n,m)\|(n,m)$ and $(n+1,\ m-1)\|(n+1,m-1)$ bisector GBs with tilts from 0° to 30°. Both types of optimal GBs are distinctly more favorable than the bisector counterparts, by up to 0.3 eV/nm within our limited model size. The optimal GBs are also featured by the suppressed warping with amplitude of merely ~0.2 Å in both the graphene and BN domains (Fig. 5, left inset), signifying that the in-plane strains have been eliminated and the GB energy is dominated by the 5|7 dislocations, i.e. $E_{GB}=E_{5|7s}$. Once the GB is decoupled from its neighbors, its energy does not change with further increasing domain size. In contrast, in the bisector GB the BN domain displays remarkable warping with amplitude up to 1.1 Å due to interface-imposed compressive strain (Fig. 5, right inset); the warping amplitude near the GBs is also enhanced due to synergic effect of mismatch strain and dislocations. Since the deformation in graphene and BN domains is dominated by stretching and warping, respectively, the energy of a bisector GB can be analytically approximated as

$$E_{GB}=E_{5|7s}+\frac{1}{2}A_{gr}E_{gr}\varepsilon_{gr}^2+\frac{1}{2}A_{BN}\kappa_{BN}\rho_{BN}^2, \tag{9}$$

where E_{gr} is the Young's modulus of graphene (normalized over thickness), κ_{BN} is the bending stiffness of BN sheet, ε_{gr} is the tensile strain in graphene domain, ρ_{BN} is the averaged warping curvature in BN domain, and A_{gr} and A_{BN} are the corresponding domain areas. Eq. (9) displays that the energy gain by forming the optimal GBs will rise even higher with increasing domain size, without saturation effect due to the non-decaying feature of ε_{gr} and ρ_{BN}. Moreover, as both ε_{gr} and ρ_{BN} are proportional to lattice mismatch ε, the energy gain increases quadratically with ε; and the optimal GBs in the corresponding 2D materials will be much more beneficial.

5. Conclusions

In summary, our intensive theoretical analyses have revealed a new paradigm of grain boundaries in hybrid 2D materials that lifts the lattice mismatch and releases the in-plane strain. In contrast to the bisector grain boundaries preferred in homogenous 2D materials, the optimally matched grain boundaries in hybrid materials will deviate from the bisector line. We have derived a general formula to describe the interdependence of structural parameters for the optimal grain boundaries, showing that a larger tilt grain boundary tends to have longer periodic length but smaller deviation angle from the bisector line; increasing the lattice mismatch shortens the periodic length yet enlarges the deviation angle. The ground state structures of the optimal grain boundaries are proved to be a series of misaligned bisector segments that laterally shift one-by-one by halflattice constant, which are further confirmed by first-principle calculations. Furthermore, the dislocations in grain boundaries tend to locate at the hybrid interface as a result of strong attractive interaction in-between, and they are likely to be composed of N-rich pentagon and B-rich heptagon in the case of 2D BNC sheets. These results not only enrich

the knowledge of grain boundaries but also serve an essential step-stone for further exploring applications of various hybrid 2D materials.

Acknowledgments

This work was supported by the Department of Energy, BES (Grant no. ER46598). The computations were performed at the NERSC, supported by the Office of Science of the DOE under Contract No. DE-AC02-05CH11231.

Appendix A. Supporting information

Supplementary data associated with this article can be found in the online version at http://dx.doi.org/10.1016/j.jmps.2014.05.009.

References

Ajayan, P.M., Yakobson, B.I., 2011. Graphene: pushing the boundaries. Nat. Mater. 10, 415–417.
An, J., Voelkl, E., Suk, J.W., Li, X., Magnuson, C.W., Fu, L., Tiemeijer, P., Bischoff, M., Freitag, B., Popova, E., Ruoff, R.S., 2011. Domain (grain) boundaries and evidence of "twinlike" structures in chemically vapor deposited grown graphene. ACS Nano 5, 2433–2439.
Balog, R., Jorgensen, B., Nilsson, L., Andersen, M., Rienks, E., Bianchi, M., Fanetti, M., Laegsgaard, E., Baraldi, A., Lizzit, S., Sljivancanin, Z., Besenbacher, F., Hammer, L., Pedersen, T.G., Hofmann, P., Hornekaer, L., 2010. Bandgap opening in graphene induced by patterned hydrogen adsorption. Nat. Mater. 9, 315–319.
Bhowmick, S., Singh, A.K., Yakobson, B.I., 2011. Quantum dots and nanoroads of graphene embedded in hexagonal boron nitride. J. Phys. Chem. C 115, 9889–9893.
Castro Neto, A.H., Guinea, F., Peres, N.M.R., Novoselov, K.S., Geim, A.K., 2009. The electronic properties of graphene. Rev. Mod. Phys. 81, 109–162.
Chang, T., Gao, Huajian, 2003. Size-dependent elastic properties of a single-walled carbon nanotube via a molecular mechanics model. J. Mech. Phys. Solids 51, 1059–1074.
Chang, T., Geng, J., Guo, X., 2006. Prediction of chirality- and size-dependent elastic properties of single-walled carbon nanotubes via a molecular mechanics model. Proc. R. Soc. A 462, 2523–2540.
Ci, L., Song, L., Jin, C., Jariwala, D., Wu, D., Li, Y., Srivastava, A., Wang, Z.F., Storr, K., Balicas, L., Liu, F., Ajayan, P.M., 2010. Atomic layers of hybridized boron nitride and graphene domains. Nat. Mater. 9, 430–435.
da Rocha Martins, J., Chacham, H., 2010. Disorder and segregation in B−C−N graphene-type layers and nanotubes: tuning the band gap. ACS Nano 5, 385–393.
Ding, Y., Wang, Y., Ni, J., 2009. Electronic properties of graphene nanoribbons embedded in boron nitride sheets. Appl. Phys. Lett. 95, 123105.
Dutta, S., Manna, A.K., Pati, S.K., 2009. Intrinsic half-metallicity in modified graphene nanoribbons. Phys. Rev. Lett. 102, 096601.
Gao, Y., Zhang, Y., Chen, P., Li, Y., Liu, M., Gao, T., Ma, D., Chen, Y., Cheng, Z., Qiu, X., Duan, W., Liu, Z., 2013. Toward single-layer uniform hexagonal boron nitride–graphene patchworks with zigzag linking edges. Nano Lett. 13, 3439–3443.
Geim, A.K., Novoselov, K.S., 2007. The rise of graphene. Nat. Mater. 6, 183–191.
Gibb, A.L., Alem, N., Chen, J.-H., Erickson, K.J., Ciston, J., Gautam, A., Linck, M., Zettl, A., 2013. Atomic resolution imaging of grain boundary defects in monolayer chemical vapor deposition-grown hexagonal boron nitride. J. Am. Chem. Soc. 135, 6758–6761.
Golberg, D., Bando, Y., Huang, Y., Terao, T., Mitome, M., Tang, C., Zhi, C., 2010. Boron nitride nanotubes and nanosheets. ACS Nano 4, 2979–2993.
Hirth, J.P., Lothe, J., 1982. In: Theory of Dislocations.
Huang, P.Y., Ruiz-Vargas, C.S., van der Zande, A.M., Whitney, W.S., Levendorf, M.P., Kevek, J.W., Garg, S., Alden, J.S., Hustedt, C.J., Zhu, Y., Park, J., McEuen, P.L., Muller, D.A., 2011. Grains and grain boundaries in single-layer graphene atomic patchwork quilts. Nature 469, 389–392.
Jiang, L., Guo, W., 2011. A molecular mechanics study on size-dependent elastic properties of single-walled boron nitride nanotubes. J. Mech. Phys. Solids 59, 1204–1213.
Jin, C., Lin, F., Suenaga, K., Iijima, S., 2009. Fabrication of a freestanding boron nitride single layer and its defect assignments. Phys. Rev. Lett. 102, 195505.
Jung, J., Qiao, Z., Niu, Q., MacDonald, A.H., 2012. Transport properties of graphene nanoroads in boron nitride sheets. Nano Lett. 12, 2936–2940.
Kim, K., Lee, Z., Regan, W., Kisielowski, C., Crommie, M.F., Zettl, A., 2011. Grain boundary mapping in polycrystalline graphene. ACS Nano 5, 2142–2146.
Kresse, G., Furthmüller, J., 1996. Efficient iterative schemes for ab initio total-energy calculations using a plane-wave basis set. Phys. Rev. B 54, 11169–11186.
Kresse, G., Hafner, J., 1994. Ab initio molecular-dynamics simulation of the liquid-metal-amorphous-semiconductor transition in germanium. Phys. Rev. B 49, 14251–14269.
Lee, C., Wei, X., Kysar, J.W., Hone, J., 2008. Measurement of the elastic properties and intrinsic strength of monolayer graphene. Science 321, 385–388.
Liu, Y., Yakobson, B.I., 2010. Cones, pringles, and grain boundary landscapes in graphene topology. Nano Lett. 10, 2178–2183.
Liu, Y., Bhowmick, S., Yakobson, B.I., 2011. BN white graphene with "colorful" edges: the energies and morphology. Nano Lett. 11, 3113–3116.
Liu, Y., Wu, X., Zhao, Y., Zeng, X.C., Yang, J., 2011. Half-metallicity in hybrid graphene/boron nitride nanoribbons with dihydrogenated edges. J. Phys. Chem. C 115, 9442–9450.
Liu, Y., Zou, X., Yakobson, B.I., 2012. Dislocations and grain boundaries in two-dimensional boron nitride. ACS Nano 6, 7053–7058.
Liu, Z., Ma, L., Shi, G., Zhou, W., Gong, Y., Lei, S., Yang, X., Zhang, J., Yu, J., Hackenberg, K.P., Babakhani, A., Idrobo, J.-C., Vajtai, R., Lou, J., Ajayan, P.M., 2013. In-plane heterostructures of graphene and hexagonal boron nitride with controlled domain sizes. Nat. Nanotechnol. 8, 119–124.
Lu, P., Zhang, Z., Guo, W., 2010. Magnetism in armchair BC2N nanoribbons. Appl. Phys. Lett. 96, 133103.
Lu, P., Zhang, Z., Guo, W., 2011. Electronic structures of BC2N nanoribbons. J. Phys. Chem. C 115, 3572–3577.
Muchharla, B., Pathak, A., Liu, Z., Song, L., Jayasekera, T., Kar, S., Vajtai, R., Balicas, L., Ajayan, P.M., Talapatra, S., Ali, N., 2013. Tunable electronics in large-area atomic layers of boron–nitrogen–carbon. Nano Lett. 13, 3476–3481.
Nag, A., Raidongia, K., Hembram, K.P.S.S., Datta, R., Waghmare, U.V., Rao, C.N.R., 2010. Graphene analogues of BN: novel synthesis and properties. ACS Nano 4, 1539–1544.
Novoselov, K.S., Jiang, D., Schedin, F., Booth, T.J., Khotkevich, V.V., Morozov, S.V., Geim, A.K., 2005. Two-dimensional atomic crystals. Proc. Natl. Acad. Sci. 102, 10451–10453.
Ramasubramaniam, A., Naveh, D., 2011. Carrier-induced antiferromagnet of graphene islands embedded in hexagonal boron nitride. Phys. Rev. B 84, 075405.
Ranganathan, S., 1996. On the geometry of coincidence-site lattices. Acta Crystallogr. 21, 197–199.
Sutter, P., Cortes, R., Lahiri, J., Sutter, E., 2012. Interface formation in monolayer graphene–boron nitride heterostructures. Nano Lett. 12, 4869–4874.
Wei, Y., Wu, J., Yin, H., Shi, X., Yang, R., Dresselhaus, M., 2012. The nature of strength enhancement and weakening by pentagon–heptagon defects in graphene. Nat. Mater. 11, 759–763.

Wu, J., Wei, Y., 2013. Grain misorientation and grain-boundary rotation dependent mechanical properties in polycrystalline graphene. J. Mech. Phys. Solids 61, 1421–1432.
Yazyev, O.V., Louie, S.G., 2010. Electronic transport in polycrystalline graphene. Nat. Mater. 9, 806–809.
Yu, Q., Jauregui, L.A., Wu, W., Colby, R., Tian, J., Su, Z., Cao, H., Liu, Z., Pandey, D., Wei, D., Chung, T.F., Peng, P., Guisinger, N.P., Stach, E.A., Bao, J., Pei, S.-S., Chen, Y.P., 2011. Control and characterization of individual grains and grain boundaries in graphene grown by chemical vapour deposition. Nat. Mater. 10, 443–449.
Zhang, Y., Tan, Y.-W., Stormer, H.L., Kim, P., 2005. Experimental observation of the quantum Hall effect and Berry's phase in graphene. Nature 438, 201–204.
Zhang, Z., Guo, W., 2008. Energy-gap modulation of BN ribbons by transverse electric fields: first-principles calculations. Phys. Rev. B 77, 075403.